

Ensemble Characteristics of the ZZ Ceti stars

Anjum S. Mukadam¹

Department of Astronomy, University of Washington, Seattle, WA - 98195-1580, U.S.A.;
anjum@astro.washington.edu

M. H. Montgomery, D. E. Winget

Department of Astronomy, University of Texas at Austin, Austin, TX - 78712, U.S.A.

S. O. Kepler

Instituto de Física, Universidade Federal do Rio Grande do Sul, 91501-970 Porto Alegre,
RS - Brazil.

J. C. Clemens

Department of Physics and Astronomy, University of North Carolina, Chapel Hill, NC
27599, U.S.A.

ABSTRACT

We present the observed pulsation spectra of all known non-interacting ZZ Ceti stars (hydrogen atmosphere white dwarf variables; DAVs) and examine changes in their pulsation properties across the instability strip. We confirm the well established trend of increasing pulsation period with decreasing effective temperature across the ZZ Ceti instability strip. We do not find a dramatic order of magnitude increase in the number of observed independent modes in ZZ Ceti stars, traversing from the hot to the cool edge of the instability strip; we find that the cool DAVs have one more mode on average compared to the hot DAVs. We confirm the initial increase in pulsation amplitude at the blue edge, and find strong evidence of a decline in amplitude prior to the red edge. We present the first observational evidence that ZZ Ceti stars lose pulsation energy just before pulsations shut down at the empirical red edge of the instability strip.

Subject headings: stars:oscillations—stars: variables: other—white dwarfs

¹Hubble Fellow

1. Introduction

Asteroseismology is the only systematic technique to study the insides of a star. Pulsators are fortunately found all over the H-R diagram, and allow us the opportunity to look inside different stars in various evolutionary stages. White dwarf stars are the stellar remains of 98–99% of stars in the sky (Weidemann 1990), and contain an archival record of their main sequence lifetime. Pulsating white dwarf stars serve as effective instruments to harness this archival record.

White dwarf spectra reveal that 80% of them have atmospheres dominated by hydrogen (DAs; Fleming et al. 1986). Hydrogen atmosphere DA white dwarfs are observed to pulsate in an instability strip located in the temperature range 10800–12500 K for $\log g \approx 8$ (Bergeron et al. 1995, 2004; Koester & Allard 2000; Koester & Holberg 2001; Mukadam et al. 2004b). Recent studies determine that the DA instability strip is only about 1000–1200 K in width (Mukadam et al. 2004b; Gianninas et al. 2005). These DA variables (DAVs) are known as the ZZ Ceti stars, after the proto type ZZ Ceti (R 548) of the class.

In this paper we gather the pulsation spectra of all known non-interacting ZZ Ceti stars with the purpose of studying their ensemble pulsation characteristics, and how these properties change across the instability strip. Such a systematic study of the ZZ Ceti pulsators was first undertaken by pioneers in the field such as Robinson (1980), McGraw et al. (1981), and Winget & Fontaine (1982). Clemens (1993) was the first to demonstrate the distinct behavior of pulsation periods and amplitudes as a function of temperature systematically for a significant sample of DAVs. The sample size of known DAVs is now three times larger than the sample used in the last such characterization of the ZZ Ceti pulsators by Kanaan et al. (2002).

Also, we now have better and internally consistent temperatures for these pulsators, calculated using the $ML2/\alpha = 0.6$ convection description (see Bergeron et al. 2004; Kleinman et al. 2004). This prescription for convection gives the best internal consistency between optical and ultra-violet (UV) effective temperatures, trigonometric parallaxes, V magnitudes, and gravitational redshifts (Bergeron et al. 1995; Koester & Vauclair 1997; Bergeron & Lamontagne 2003; Fontaine et al. 2003). These two reasons compel us to re-examine the pulsation characteristics of the instability strip.

1.1. Defining our ZZ Ceti samples

Of the 35 new ZZ Ceti variables published in Mukadam et al. (2004a), HS0951+1312, HS0952+1816, WD1443+0134, WD1524-0030, and WD2350-0054 do not have reliable spec-

troscopic T_{eff} and $\log g$ fits (see Mukadam et al. 2004a,b). Our sample of new ZZ Ceti variables discovered using spectra from the Sloan Digital Sky Survey (SDSS) then consists of 30 DAVs from Mukadam et al. (2004a) and 11 DAVs from Mullally et al. (2005). For these 41 DAVs, D. Eisenstein derived a homogeneous and internally consistent set of T_{eff} and $\log g$ values from the SDSS using model atmospheres from D. Koester (see Kleinman et al. 2004). We carefully and consistently re-analyzed all of our time-series photometry data on these pulsators, acquired using the prime focus CCD camera Argos (Nather & Mukadam 2004) on the 2.1 m telescope at McDonald Observatory. We shall henceforth refer to this set of 41 DAVs as the SDSS ZZ Ceti sample with homogeneous spectroscopic fits and homogeneous time-series photometry.

Bergeron et al. (2004) and Gianninas et al. (2005) have published internally consistent temperatures and $\log g$ fits for 39 DAVs using their latest model atmospheres; we will henceforth refer to this second set of 39 DAVs as the BG04 ZZ Ceti sample. We compiled a corresponding set of 39 pulsation spectra from the literature, and via private communication with our colleagues. The seismic data of the BG04 ZZ Ceti sample was acquired by different observers using different instruments and telescopes. However a substantial amount of time-series data exists on most DAVs in this sample, and we utilized practically all published pulsation spectra to carefully derive well-averaged values of weighted mean period and pulsation amplitudes which we present in this paper.

Mukadam et al. (2004b) show evidence of a relative shift of about 200 K between the SDSS and BG04 ZZ Ceti instability strips, which also differ in shape and width. The spectra of ZZ Ceti stars in these samples were analyzed using different techniques and with different model atmospheres. As homogeneity is imperative, we cannot merge these two samples for analyses that involve the spectroscopic temperature. However we can merge these two samples when formulating plots based solely on seismic data such as Figure 3.

During the writing of this manuscript, 25 new ZZ Ceti stars were submitted for publication in separate papers: Silvotti et al. 2005a, Castanheira et al. 2005, Kepler et al. 2005b, Gianninas et al. 2005, and Silvotti et al. 2005b. This brings the total number of non-interacting ZZ Ceti stars known to 107. Twenty of the new DAVs in these papers come from the SDSS. Their spectroscopic T_{eff} and $\log g$ values were derived using the same technique as the 41 SDSS DAVs discovered previously, but with a different algorithm (version auto23 vs. auto21 used earlier). Hence we cannot include the new DAVs in our SDSS ZZ Ceti sample for plots based on effective temperature, such as Figures 1 and 2. Also, we find that the main purpose of the pulsation spectra presented in these papers is to demonstrate discovery of variability. Such pulsation spectra may be incomplete and are not well suited for direct

inclusion in most plots of this paper where ensemble homogeneity plays a big role². However we will include these variables in Figure 3 (based on seismic data) for completeness, and show the net effect of the inclusion on the original plot.

1.2. Methodology: using only linearly independent pulsation frequencies

Brickhill (1992), Brassard et al. (1995), Wu (2001), and ? show that the non-linear pulse shapes observed in some variable white dwarfs may arise as a result of relatively thick convection zones. Many frequencies are evident in these stars because the non-linearities appear as harmonics and linear combinations in our Fourier transforms. We are interested in studying the pulsation characteristics of self-excited real modes in the context of this paper. Hence we will disregard all harmonics and linear combination frequencies in the observed pulsation spectra throughout this paper.

When our program detects a linear combination or harmonic in an observed pulsation spectrum, we typically hand-pick the lowest amplitude mode as the linear combination mode. However if we find a mode involved in two or more linear combinations, we consider it to be a linear combination mode even if it is not the lowest amplitude mode. Our simplistic approach could lead us to incorrect choices; we could be misinterpreting resonances as linear combination modes in a few cases. However any small discrepancies in values evaluated for a single star should have a minimal impact on the conclusions we draw from the ensemble.

2. Changes in pulsation properties across the ZZ Ceti instability strip

Short pulsation periods (100–300 s) in the ZZ Ceti stars typically have pulsation amplitudes of a few percent or smaller. Long pulsation periods (600–1000 s) typically have large amplitudes that can be as high as 10%. This correlation between the pulsation periods and amplitudes of the ZZ Ceti stars has been established for a long time (Robinson 1979, 1980; McGraw 1980; Fontaine et al. 1982). However the correlation of these properties with temperature had to wait more than a decade for sufficiently accurate determinations of ZZ Ceti temperatures. Subsequently the distinct behavior of pulsation periods and amplitudes as a function of temperature was systematically demonstrated for a significant sample of DAVs

²We added three new DAVs HS1039+4112 (?), G232-38 (Gianninas et al. 2005), and GD133 (Silvotti et al. 2005b) to the original BG04 sample of 36 stars; this does not significantly affect the homogeneity of the BG04 sample as the new DAVs constitute less than 10% of the sample. However adding 20 new SDSS DAVs to the SDSS ZZ Ceti sample of 41 stars would significantly affect the homogeneity of the sample.

by Clemens (1993) and more recently by Kanaan et al. (2002). We now demonstrate and discuss these trends for the new as well as previously known DAVs of our two homogeneous samples. We will begin with showing how the number of observed independent modes changes across the instability strip.

2.1. Number of observed independent modes

We expect a larger (than intrinsic) scatter in the number of independent modes we measure for an ensemble of ZZ Ceti stars due to varied detection efficiency. This partially arises because we use different instruments on different telescopes, or observe for different durations of time, and also due to the variety of weather conditions and extinction values. A fraction of the scatter in our detection efficiency is caused because ZZ Ceti stars have different magnitudes and different pulsation amplitudes, and the pulsation amplitudes depend on the effective wavelength of observation (Robinson et al. 1982).

By using the SDSS ZZ Ceti sample alone, we reduce some of this expected scatter (see subsection 1.1). To reduce the scatter additionally, we choose to limit ourselves to the magnitude range $17.8 \leq g \leq 18.8$ and to a stellar mass $M_{\odot} < 1.0 M_{\odot}$ to exclude intrinsic low amplitude DAVs (see section 2.3). Reducing our magnitude range any more will take us further into the realm of small number statistics. For the subset of 23 SDSS DAVs that fall in the chosen range, we find an average of 2.5 modes/star for the hotter ZZ Ceti stars (11300–11800 K), and a slightly larger value of 3.1 modes/star for the cooler ZZ Ceti stars (10800–11300 K). If we consider all the SDSS DAVs in our sample, excluding the three massive variables (WD0923+0120, WD1711+6541, & WD2159+1322), then we find an average of 2.9 modes/star for the hotter ZZ Ceti stars (11300–11800 K) and 3.3 modes/star for the cooler ZZ Ceti stars (10800–11300 K) up to an amplitude limit of order a few mma. This may seem contrary to published literature, but we are attempting to restrict ourselves to independent self-excited modes only, rather than plot the total number of observed periodicities in the star.

The period spacing for nonradial g-modes with $k \leq 3$ is larger than the asymptotic limit. This increase in the density of available eigenmodes as a function of period is consistent with the increase we find in the number of observed independent modes, comparing the hotter ZZ Ceti stars to the cooler ZZ Ceti stars.

2.2. Observed pulsation periods

Pulsations in ZZ Ceti models (and in stars in general) are self-driven oscillations. Stochastic noise frequencies coincident with the eigenfrequencies are amplified by the driving mechanism to observable amplitudes. The blue edge of the ZZ Ceti instability strip occurs when the star is cool enough to have a hydrogen partial ionization zone sufficiently deep to excite global pulsations.

Our models suggest that the driving frequency is governed by the thermal timescale at the base of the hydrogen partial ionization zone (see Cox 1980; Unno et al. 1989). As the model star cools, the base of the partial ionization zone moves deeper in the model, and the thermal timescale increases (Winget 1982; Hansen et al. 1985). Numerical calculations by Montgomery (2005) show that the thermal timescale at the base of the ionization zone τ_{th} is proportional to T_{eff}^{-90} . However recent investigations by Kim et al. (2005) suggest that the thermal timescale is not consistent with the mean pulsation period, although both quantities increase in the models as we traverse from the blue to the red edge of the instability strip.

Figure 1 shows the mean pulsation period as a function of effective temperature for DAVs in both the SDSS and BG04 ZZ Ceti samples. We determine the Weighted Mean Period (WMP) for each DAV by weighting each period with the corresponding observed amplitude (see equation 1).

$$\text{Weighted Mean Period (WMP)} = \frac{\sum_i P_i A_i}{\sum_i A_i} \quad (1)$$

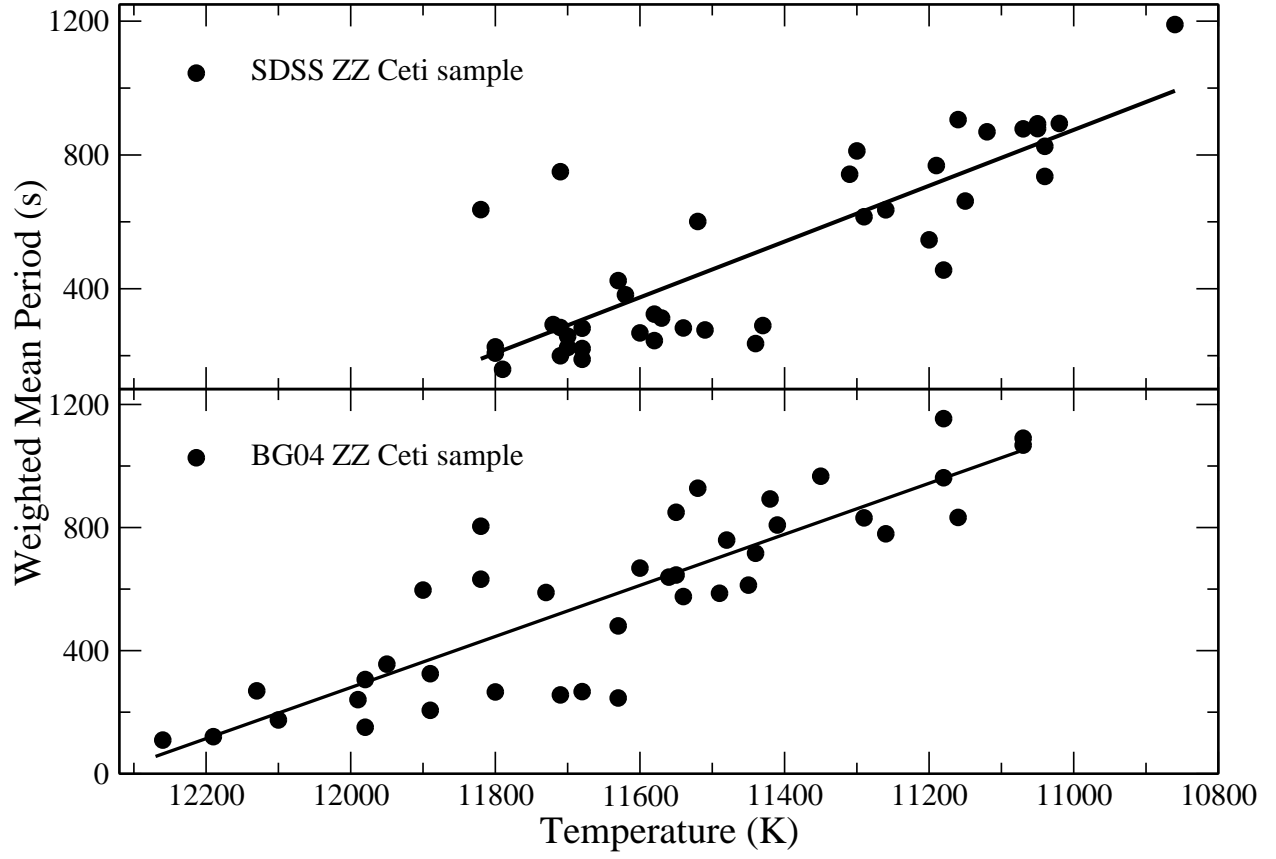


Fig. 1.— We show the weighted mean period of 41 newly discovered ZZ Ceti stars from the SDSS (top) and 39 ZZ Ceti stars from the BG04 sample (bottom) vs their spectroscopic temperature; each period was weighted by the observed amplitude. We note the distinct increase in mean pulsation period as DAVs cool across the ZZ Ceti instability strip.

We can now appreciate the significance of Figure 1; the weighted mean pulsation period provides us with a method of determining the temperature of a ZZ Ceti star independent of spectroscopy. The respective equations of the best fit lines through the SDSS and the BG04 ZZ Ceti samples shown in Figure 1 are:

$$\begin{aligned} \text{WMP}_{\text{SDSS}} &= -0.835^{\pm 0.089} \times T_{\text{effSDSS}} + 10060^{\pm 1020} \\ \text{WMP}_{\text{BG04}} &= -0.830^{\pm 0.079} \times T_{\text{effBG04}} + 10240^{\pm 920} \end{aligned}$$

where WMP is in units of seconds and T_{eff} is in units of Kelvin. It is reassuring to see an agreement in the values of the slope for both the SDSS and BG04 ZZ Ceti samples, and gives us more confidence in using this period-temperature correlation as a means to measure the effective temperature of a DAV. We can now determine a temperature for the five variables with unreliable spectroscopic fits we excluded earlier, HS0951+1312, HS0952+1816, WD1443+0134, WD1524-0030, and WD2350-0054 (see Table 1 in the appendix).

We compute a sum of the squares of the **horizontal** offsets of the points in Figure 1 respectively from the above best fit lines, and arrive at a seismic estimate of the average uncertainty in our spectroscopic temperature. We determine $\sigma_{T_{\text{eff}}} = 188.3 \text{ K}$ for the SDSS ZZ Ceti sample, and $\sigma_{T_{\text{eff}}} = 185.4 \text{ K}$ for the BG04 ZZ Ceti sample. It is not surprising that the average T_{eff} uncertainties in both these samples turned out to be similar because ZZ Ceti stars in both samples define an instability strip of the same width $\sim 1000\text{--}1200 \text{ K}$ (Mukadam et al. 2004b; Gianninas et al. 2005). We can expect that if the average T_{eff} uncertainty in the SDSS sample had been significantly larger than that of the BG04 sample, the empirical width of the SDSS instability strip would also have been correspondingly larger.

Our current temperature determinations are getting better and may be internally consistent to about 200 K at present. Our empirical measure of the width of the instability strip appears to have reduced from 1500 K (Bergeron et al. 1995; Koester & Allard 2000) to about 1000–1200 K (Mukadam et al. 2004b; Gianninas et al. 2005). But even with our current atmospheric models we do find exceptions to this period- T_{eff} correlation, where the spectroscopic temperature does not match the pulsation properties of the ZZ Ceti star. For example, Mukadam et al. (2004a,b) report the ZZ Ceti star WD2350-0054 with a dominant period close to 300 s as an unusual pulsator because its SDSS spectroscopic determination places it below the red edge of the instability strip at $T_{\text{eff}} = 10350 \pm 60 \text{ K}$. Bergeron et al. (2004) report a known complex pulsator G29-38 (Kleinman et al. 1998) as a hot ZZ Ceti star with $T_{\text{eff}} = 11820 \text{ K}$. Better S/N spectra of these and other such ZZ Ceti stars may reveal temperatures consistent with their observed periods. Unless the pulsation characteristics themselves reveal curious features, it seems premature to conclude that the ZZ Ceti star in question (with a spectroscopic temperature inconsistent with its pulsation spectrum) is strange or abnormal in any way.

2.2.1. *Weighted Mean Period as a temperature indicator*

Measuring the pulsation periods of a ZZ Ceti star is a model-independent and straight forward process³ as opposed to a spectroscopic determination of its temperature. The instability strip spans 1000–1200 K in temperature and about 1300 s in period. The internal uncertainty in measuring temperature using spectra is typically about 200 K, which is 17–20% of the width of the instability strip. While even low quality photometric data will yield a period precise to at least a few seconds. For the hotter ZZ Ceti stars, with little or no amplitude modulation, the uncertainty in WMP constitutes less than 1% of the width of the instability strip in period. Cooler ZZ Ceti stars with a significant amplitude modulation can exhibit pulsation spectra with a WMP different by 30–60 s and in a few cases even as much as 100–200 s. For most of the cooler ZZ Ceti stars, the uncertainty in WMP represents less than 5% of the width of the instability strip⁴. We therefore expect that this method of using the WMP to effectively measure the location of a DAV within the instability strip is in general more accurate and reliable than spectroscopy.

Any dispersion in period due to differences in stellar mass, core composition, H/He layer masses, etc., can increase the uncertainty of determining the temperature of a given DAV using this relation. We expect this may be significantly smaller than our present typical spectroscopic T_{eff} uncertainties of a few 100 K.

Note that we do not claim that the relationship between the WMP and the temperature is linear; a straight line is merely the simplest model fit possible to the observations shown in Figure 1, considering the large amount of scatter. We do not necessarily require a linear relation between WMP and T_{eff} for this method to work as a temperature indicator. Our collaborators at the University of Texas are presently investigating the interpretation of these data in terms of the theoretical models (Kim et al. 2006; in preparation).

The plot of WMP vs. T_{eff} is similar to comparing two independent temperature scales, each with its own independent source of uncertainties. The uncertainty in spectroscopic T_{eff} depends on the quality of the spectrum, the accuracy and completeness of the model atmosphere, and the details of the algorithm used to fit the observed spectrum with the

³While it is true that aliases complicate the determination of pulsation periods from single site data, this ambiguity may change the value of the period typically by only a few seconds.

⁴G29-38 is the only example we find in the literature where the published pulsation spectra exhibit a change in WMP by 375 s (see McGraw & Robinson 1975; Kleinman 1995; Kleinman et al. 1998). It is a complex pulsator with a spectroscopic temperature of a hot ZZ Ceti star (Bergeron et al. 2004); its large amplitude probably indicates a temperature excursion of up to 500 K, a substantial part of the instability strip. It seems difficult to determine a reliable effective temperature of G29-38 by either method.

template spectra. Large amplitude variables have a corresponding higher uncertainty in temperature (McGraw 1979). The uncertainty in WMP comes from the quality of the photometric observations, and the amplitude modulation of the star.

As long as we restrict our relative T_{eff} parameter in units of seconds in the WMP temperature scale, the uncertainty in our measurements is not related to spectroscopic temperature values at all. It is only when we attempt to translate WMP into a temperature in degree Kelvin, that we have to use the relation between WMP and spectroscopic temperature. Even in this case, we are still better off than the typical 200 K uncertainty in spectroscopic temperature because the slopes of the best fit lines in Figure 1 do not depend on a few stars, but on 35–40 stars. Using WMP directly as a temperature scale is non-intuitive at the present time. But this maybe worth thinking about as an alternative scale in the long run, once we improve our understanding of the relation between WMP and T_{eff} , both observationally and theoretically.

2.2.2. Re-defining the ZZ Ceti classification

We presently classify the ZZ Ceti stars into two groups: the hot DAVs and the cool DAVs. However a clear dividing point (in temperature) between these two classes does not exist to date in published literature. Our present classification of these stars is thus vague in this context, although it has certainly proved to be a useful guide. The primary reason such a temperature based classification cannot be well defined is because the location and width of the instability strip are model-dependent features. Model atmospheres of DAV stars treat convection with some parameterization, the choice of which can shift the instability strip in temperature by a few thousand K (Bergeron et al. 1995; Koester & Allard 2000).

The pulsation characteristics of the ZZ Ceti stars helped us divide them into simple and complex pulsators in the late seventies. A decade later, we recognized that the simple pulsators that exhibit a few modes with short periods (200–300 s), small amplitudes (few mma), sinusoidal or saw-toothed pulse shapes, and continued to show the same pulsation spectra over a few decades, were hot ZZ Ceti stars. We also realized that the complex pulsators that exhibit several long periods (600–1200 s) with large amplitudes (40–110 mma), non-sinusoidal pulse shapes with fast rise times and slow decadence, and amplitude modulation over timescales of a few days to a few years, were cool ZZ Ceti stars. Although we now use spectroscopic temperature as a means to classify these stars, the classification scheme came about only because we initially used the pulsation characteristics to separate these stars into two groups.

We suggest a new ZZ Ceti classification scheme based on the WMP of these variables. We intend to retain the fundamental aspect of the previous scheme in using a temperature based classification. We have shown that WMP is also a temperature scale (Figure 1). We expect that WMP serves as a more accurate and reliable T_{eff} scale than spectroscopic temperature because measuring the pulsation periods of a ZZ Ceti star constitutes a relatively simple, less uncertain, and model-independent exercise compared to measuring its spectroscopic temperature.

We redefine the class of hot DAVs (hDAVs) as ZZ Ceti stars with $\text{WMP} < 350\text{ s}$. We redefine the class of cool DAVs (cDAVs) as ZZ Ceti stars with $\text{WMP} > 650\text{ s}$. We suggest introducing a new class of DAVs, to be called the intermediate DAVs (iDAVs), as ZZ Ceti stars with $350 \leq \text{WMP} \leq 650$. This class merely forms the evolutionary subclass adjoining the hot and cool ZZ Ceti stars and typically encompasses those ZZ Ceti pulsators that show a large range of pulsation periods, e.g. HS0507+0435B.

For borderline cases such as G29-38, when one season of observations place the DAV in one class, and a second season places it in another class, then we suggest choosing the coolest class of the two possibilities. We find several cases where a cDAV or an iDAV exhibit modes typical of the hotter pulsators, but we have not seen an instance of a hot DAV exhibiting a mode typical of the cool ZZ Ceti stars. We show our suggested classification for most of the known non-interacting ZZ Ceti stars in Tables 1 and 2.

Note that the boundaries of 350 s and 650 s are arbitrary in some sense; we merely wished to divide the instability strip into three parts and used a period histogram to fine-tune our choice. For simplicity and better readability, Tables 1 and 2 in the appendix do not show all of the pulsation spectra we accrued for each star. We show multiple seasons of observations only for those DAVs that exhibit different frequencies and amplitudes at different times. This also helps us understand the intrinsic changes in weighted mean period and mean pulsation amplitude for such variables. To use such stars in the ensemble, we computed the weighted mean period and mean pulsation amplitude for each season of observations individually, and then included the average value in our analysis. We refer the reader to ?, Castanheira et al. (2005), ?, Gianninas et al. (2005), and Silvotti et al. (2005b) for the pulsation spectra of the new DAVs.

2.3. Observed pulsation amplitudes

The physical quantity of interest in this subsection is the intrinsic pulsation amplitude of modes excited in the ZZ Ceti star. But the measured amplitudes of observed modes are

most likely lower than the intrinsic amplitudes due to geometric cancellation. This effect has three independent causes: disk averaging, inclination angle, and limb darkening. We are unable to resolve the disk of the star from Earth. Hence the observed amplitude of each pulsation mode is lower due to a disk-averaging effect. This explains why the probability of detecting $\ell=1$ modes is higher than the detection probability for $\ell=2$ and $\ell=3$ modes. The inclination angle dictates the distribution of the bright and dark zones in our view for a given mode. Eigenmodes with different m values exhibit different cancellation patterns (see Dziembowski 1977; Pesnell 1985).

Limb darkening effectively reduces the area of the stellar disk in our view, and this reduction in area depends on wavelength. At UV wavelengths, the increased limb darkening decreases the contribution of zones near the limb. As a result, modes of higher ℓ are canceled less effectively in the UV compared to the low ℓ modes (Robinson et al. 1982). Of these three independent causes of geometric cancellation, limb darkening is the only one that works in our favor, and provides us with a mode identification technique (Robinson et al. 1995).

The intrinsic pulsation amplitude depends on the mass of the star. Nonradial g-modes have a non-negligible radial component, the amplitude of which scales with stellar mass and plays a role in dictating the amplitude of the nonradial component. The massive pulsators BPM 37093 ($\log g=8.81$), WD0923+0120 ($\log g=8.74$), WD1711+6541 ($\log g=8.64$), and WD2159+1322 ($\log g=8.61$) exhibit low amplitudes as a result of their high gravity, and hence we exclude them from section 2.3.

Figure 2 shows the square root of total power $\sqrt{(\sum_i A_i^2)}$ for 38 stars from the SDSS sample (top) and 38 stars from the BG04 ZZ Ceti sample (bottom), plotted as a function of their spectroscopic temperature. All of the pulsation amplitudes we report in this paper come from optical whole disk observations. We expect these are mostly low ℓ modes. For these reasons, we expect them to be lower than the corresponding intrinsic amplitudes due to geometric cancellation. The points that form the upper envelopes in both panels of Figure 2 are then better indicators of the intrinsic amplitude at that temperature. Note that in the few cases of under-resolved data, beating of closely spaced periodicities can lead us to determine a relatively smaller or larger amplitude than the observable amplitude.

We expect that ZZ Ceti stars with a high pulsation amplitude have a corresponding higher uncertainty in temperature. For large amplitude variables, the surface temperature changes substantially during a pulsation cycle, by as much as a thousand degrees (McGraw 1979). Depending on which phase of the pulsation cycle (typical periods of 600–1200 s for cool DAVs) we acquire the spectra and for how long, our measure of their effective temperature can be incorrect by a few hundred degrees. We can attempt to estimate this uncertainty by obtaining time-series photometry on the star simultaneous with the spectroscopic data.

At any given temperature, the apparently low amplitude variables could be suffering from extensive geometric cancellation. At the same time, the high amplitude variables with the expectedly least geometric cancellation have a proportionally high uncertainty in temperature due to the large intrinsic temperature fluctuation during a pulsation cycle. This makes the task of interpreting Figure 2 difficult. There is fortunately a silver lining to this bleak cloud: ZZ Ceti stars are multi-mode pulsators. If a ZZ Ceti with 3 independent modes still exhibits a small amplitude, then it is unlikely that we are dealing with an unfavorable inclination angle in all three cases⁵.

⁵This may not hold true if all the independent modes have the same values of ℓ and m . However we do not fully understand the mode selection mechanism for different m values. Also, they exhibit different cancellation patterns (Dziembowski 1977; Pesnell 1985).

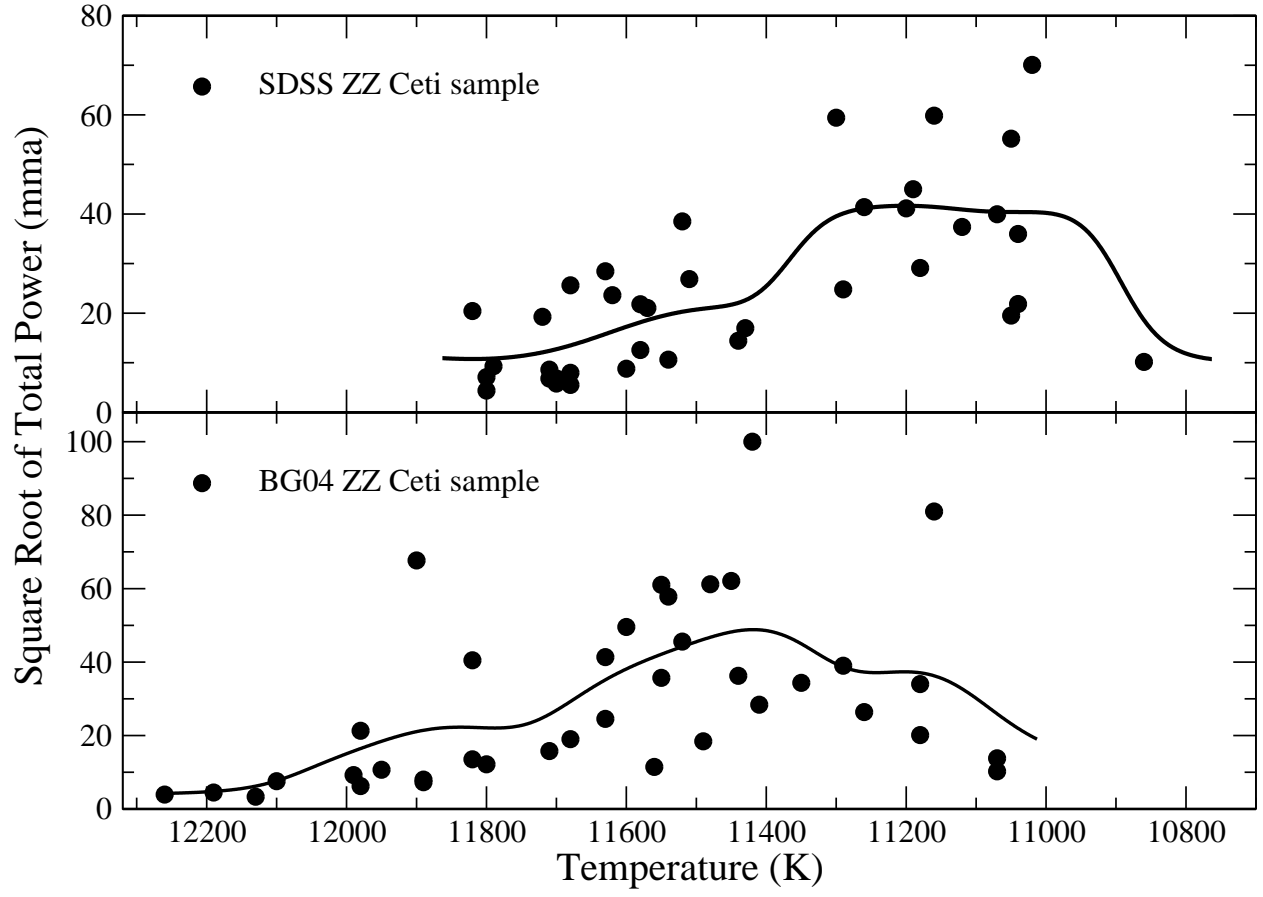


Fig. 2.— We show the square root of total power for 38 SDSS DAVs (top) and 38 DAVs from the BG04 sample (bottom) as a function of their spectroscopic temperature. The solid line shows a smooth curve obtained from Gaussian binning that demonstrates an initial increase in pulsation amplitude followed by a suggestive decline prior to the red edge.

Instead of traditional histograms, we adopt a Gaussian binning technique where each bin serves as a Gaussian function instead of a box (top-hat) function. This is a better noise averaging technique because all points contribute to the value of each bin. Although the contributions of distant points to the value of an individual bin are small, this method may not be appropriate to study sharp local trends. We are interested in slow trends across the width of the instability strip and do not hesitate to use this technique. We choose Gaussian bins with $\sigma = 75\text{ K}$ that are an infinitesimal 1 K apart from each other. We show the result as a solid line in both panels of Figure 2. Both samples show an initial increase in pulsation amplitude, and are also suggestive of a decline prior to the red edge.

We established in section 2.2 how the weighted mean pulsation period correlates directly with the effective temperature of the DAVs for both samples. We now merge both the SDSS and the BG04 samples, also including the five DAVs with unreliable spectroscopic fits (see section 1.1) to plot the pulsation amplitude as a function of the WMP. We no longer have to worry about the internal consistency in their spectroscopic temperatures, and we can use their WMP as a T_{eff} scale. We show these 81 DAVs as filled circles in Figure 3. We also include the 19 new DAVs from Silvotti et al. (2005b), Castanheira et al. (2005), and ? as filled squares. We have excluded the massive DAV WD1337+0104 ($\log g=8.55$) from ? and the low mass DAVs HE0031-5525 ($\log g=7.65$) & WD2135-0743 ($\log g=7.67$) from Castanheira et al. (2005) in Figure 3.

Figure 3 shows a plot with better statistics than Figure 2 due to the larger sample size of 100 DAVs. We used Gaussian bins of width 75 s, separated from adjacent bins by an infinitesimal amount of 1 s, to produce both the curves shown in Figure 3. The solid line is the histogram determined from the 81 average mass DAVs of the BG04 and SDSS samples, while the dotted line shows the effect of including the new 19 average mass DAVs. The minor difference between the two lines assures us that our conclusions are robust. We clearly see an initial increase in pulsation amplitude near the blue edge, followed by a gentle rise and then a decline prior to the red edge.

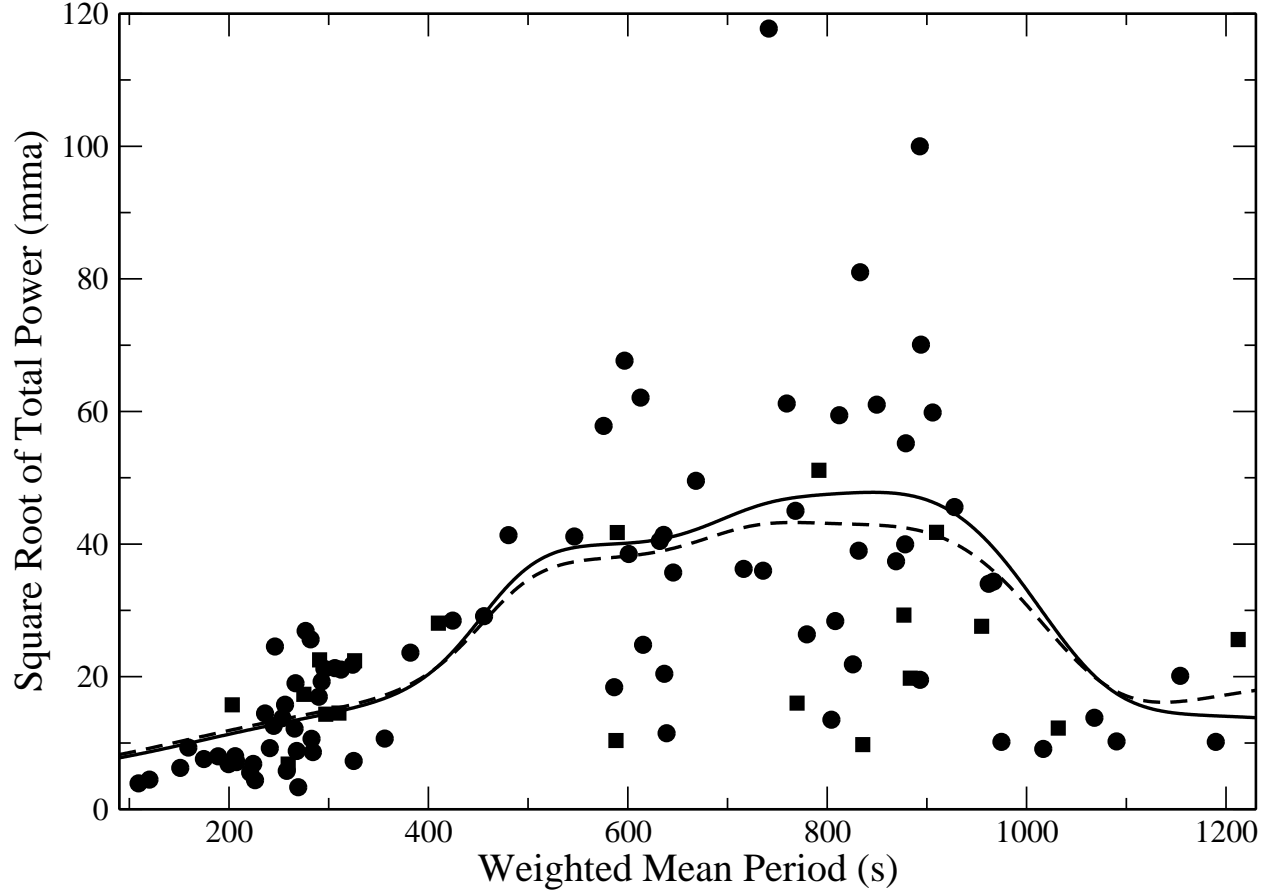


Fig. 3.— We show the square root of total power for 81 DAVs from the SDSS and BG04 samples (filled circles) and 19 newly discovered DAVs (filled squares) as a function of the weighted mean period, which is correlated to the temperature (see Figure 1). The solid line shows a histogram obtained using Gaussian bins of $\sigma=75$ s for the 81 DAVs, and the dotted line shows the effect of including the 19 new DAVs. We see an initial increase in pulsation amplitude near the blue edge, and a subsequent gentle rise followed by a decline in amplitude prior to the red edge of the ZZ Ceti instability strip.

We find several reasons why Figure 3 looks much more convincing of a decline in amplitude before the red edge compared to Figure 2. Changing from a x-axis based on spectroscopic temperature to weighted mean period allows us to include four red edge pulsators with low amplitudes, namely HS0952+1816, WD1443+0134, WD0249-0100, and WD2307-0847. Secondly, we get better statistics by combining the two samples that are individually suggestive of a decline in amplitude near the red edge. Lastly, we also find that the change in x-axis between Figures 2 and 3 moves pulsators left and right, apparently leaving behind cleaner evidence of a decline prior to the red edge. For example, we find that the low amplitude cool DAV GD 154 moves from 11180 K in Figure 2 to 1154 s in Figure 3, which corresponds to $T_{\text{eff}} \sim 10950$ K using the slope in the bottom panel of Figure 1 as a conversion factor.

We have eight pulsators with weighted mean periods of order or greater than 1000 s with amplitudes near or less than 25 mma. There are no high amplitude pulsators in this range, and the scatter in amplitude near the red edge is much smaller than the center of the ZZ Ceti instability strip. It is unlikely that unfavorable inclination angles can explain the low amplitudes of all the independent modes of all eight pulsators.

Kanaan et al. (2002) established the observed red edge at 11000 K, but did not see any decline in pulsation amplitude near the red edge within the instability strip, although they were searching for it. It is for the first time that we now have clear evidence of a decline in pulsation amplitude within the instability strip, just prior to the ZZ Ceti red edge. In other words, the star loses pulsation energy before pulsations shut down at the red edge. This work will have implications and new constraints for our pulsation models.

3. Conclusions

We find that the present large sample of non-interacting DAVs conforms to the well established trend of increasing pulsation periods with decreasing temperature across the instability strip. Investigations of the number of observed independent modes show that hot DAVs have one more mode on average compared to the cool DAVs. We also confirm the increase in pulsation amplitude near the blue edge and find strong evidence of a decline in amplitude prior to the red edge. Kanaan et al. (2002) established the observed ZZ Ceti red edge at 11000 K, but did not see any decline in pulsation amplitude near the red edge within the instability strip. We present the first observational evidence that shows the red edge is not an abrupt feature in ZZ Ceti evolution, and that the star loses pulsation energy before pulsations shut down at the red edge. This work poses new constraints on our pulsation models.

Support for this work was provided by NASA through the Hubble Fellowship grant HST-HF-01175.01-A awarded by the Space Telescope Science Institute, which is operated by the Association of Universities for Research in Astronomy, Inc., for NASA, under contract NAS 5-26555. We thank the referee for helping us make this manuscript a better paper.

Table 1. Pulsation spectra of the 41 + 5 ZZ Ceti stars mainly from the SDSS ZZ Ceti sample

Object	Class	T _{eff} (K)	log g	Linearly independent modes: Period (s) and Amplitude (mma)							
WD0018+0031 ^α	hDAV	11700	7.93	257.9	5.8						
WD0048+1521 ^α	iDAV	11290	8.23	615.3	24.8						
WD0102−0032	cDAV	11050	8.24	1043.4	15.3	926.3	34.7	830.3	35.1	752.2	19.4
WD0111+0018	hDAV	11510	8.26	292.3	21.9	255.3	15.6				
WD0214−0823	hDAV	11570	7.92	348.1	8.4	347.1	8.2	297.5	16.0	263.5	7.1
WD0318+0030	cDAV	11040	8.07	844.9	15.3	826.4	27.3	695.0	8.9	587.1	10.6
WD0332−0049	cDAV	11040	8.25	1143.7	7.4	938.4	6.7	765.0	15.2	402.0	4.1
WD0332−0049	cDAV	11040	8.25	770	23	910	10				
WD0756+2020 ^α	hDAV	11710	8.01	199.5	6.8						
WD0815+4437	iDAV	11620	7.93	787.5	7.2	311.7	18.9	309.0	10.2	258.3	6.8
WD0818+3131 ^α	hDAV	11800	8.07	253.3	2.9	202.3	3.3				
WD0825+4119	iDAV	11820	8.49	653.4	17.1	611.0	11.2				
WD0842+3707	hDAV	11720	7.73	321.1	4.4	309.3	18.0	212.3	5.2		
WD0847+4510	hDAV	11680	8.00	200.5	7.0	123.4	3.0				
WD0906−0024	iDAV	11520	8.00	769.4	26.1	618.8	9.3	574.5	23.7	457.9	9.8
WD0913+4036 ^α	hDAV	11680	7.87	320.5	14.7	288.7	12.4	260.3	16.5	203.9	3.8
WD0923+0120	cDAV	11150	8.74	655.7	4.4						
WD0923+0120	cDAV	11150	8.74	668.9	3.5						
WD0939+5609	hDAV	11790	8.22	249.9	7.2	48.5	5.9				
WD0942+5733	iDAV	11260	8.27	909.4	7.7	694.7	37.7	550.5	12.3	273.0	9.0
WD0949−0000	iDAV	11180	8.22	711.6	6.0	634.2	5.1	516.6	16.2	365.2	17.7
WD0958+0130	hDAV	11680	7.99	264.4	4.7	203.7	2.5	121.2	1.6		
WD1002+5818 ^α	hDAV	11710	7.92	304.6	5.3	268.2	6.8				
WD1007+5245 ^α	hDAV	11430	8.08	323.1	10.4	290.1	7.7	258.8	11.0		
WD1015+0306	hDAV	11580	8.14	270.0	8.4	255.7	7.3	194.7	5.8		
WD1015+5954	iDAV	11630	8.02	769.9	5.7	453.8	15.5	401.7	21.4	292.4	8.6
WD1015+5954	iDAV	11630	8.02	768.4	7.5	455.3	17.7	401.4	19.8	294.0	9.1
WD1015+5954	iDAV	11630	8.02	456.1	19.6	399.7	19.2	145.5	3.1	139.2	4.6
WD1054+5307 ^α	cDAV	11120	8.01	869.1	37.4						
WD1056−0006	cDAV	11020	7.86	1024.9	31.6	925.4	60.3	670.6	12.0	603.0	11.5
WD1122+0358	cDAV	11070	8.06	996.1	17.3	859.1	34.6	740.1	10.0		
WD1125+0345	hDAV	11600	7.99	335.1	2.8	265.8	3.3	265.5	7.1	208.6	2.8
WD1157+0553	cDAV	11050	8.15	1056.2	5.8	918.9	15.9	826.2	8.1	748.5	5.6
WD1345−0055	hDAV	11800	8.04	254.4	2.4	195.5	3.9	195.2	5.5		
WD1354+0108	hDAV	11700	8.00	322.9	1.9	291.6	2.2	198.3	6.0	173.3	1.1
WD1355+5454 ^α	hDAV	11580	7.95	324.0	21.8						
WD1417+0058	cDAV	11300	8.04	980.0	11.3	894.6	42.8	812.5	32.1	749.4	17.9
WD1502−0001	iDAV	11200	8.00	687.5	12.0	629.5	32.6	581.9	11.1	418.2	14.9
WD1617+4324	cDAV	11190	8.03	889.7	36.6	661.7	21.2	626.3	15.4		
WD1700+3549	cDAV	11160	8.04	1164.4	11.4	955.3	20.3	893.4	54.3	552.6	9.3
WD1711+6541	cDAV	11310	8.64	1248.2	3.2	690.2	3.3	606.3	5.2	234.0	1.2
WD1711+6541	cDAV	11310	8.64	1186.6	3.3	934.8	2.9	612.6	5.7	561.5	3.0
WD1724+5835	hDAV	11540	7.89	337.9	5.9	279.5	8.3	189.2	3.2		
WD1732+5905	cDAV	10860	7.99	1248.4	4.5	1122.4	8.0				
WD1732+5905	cDAV	10860	7.99	1336	7.8	1090	8.0				
WD2159+1322 ^α	cDAV	11710	8.61	801.0	15.1	683.7	11.7				
WD2214−0025 ^α	hDAV	11440	8.33	255.2	13.1	195.2	6.1				
WD1443+0134	cDAV	10830 ^β	...	1085.0	5.2	969.0	7.5				
WD1524−0030	cDAV	11160 ^β	...	873.3	110.8	717.5	28.3	498.6	21.6	255.2	17.9
WD2350−0054	hDAV	11690 ^β	...	391.1	3.1	304.1	16.3	272.8	16.2		
WD2350−0054	hDAV	11710 ^β	...	304.5	13.8	272.7	14.8	212.6	3.0		

Table 1—Continued

Object	Class	T_{eff} (K)	$\log g$	Linearly independent modes: Period (s) and Amplitude (mma)							
WD2350–0054	hDAV	11680 ^{β}	...	391.1	7.5	304.3	17.0	273.3	6.3	206.7	3.2
HS0951+1312	hDAV	11740 ^{β}	...	311.7	2.7	282.2	9.0	258.0	3.6	208.0	9.4
HS0952+1816	cDAV	10800 ^{β}	...	1160.9	7.9	945.9	10.4				
HS0952+1816	cDAV	10960 ^{β}	...	1150	4.8	883	3.6	790	2.9	674.7	3.0

^{α} We obtained the pulsation spectrum from Mullally et al. (2005).

^{β} We derived these temperatures using the best fit to the weighted mean period–spectroscopic temperature plot (Figure 1, top panel) using the first 41 SDSS DAVs listed in this table.

Table 2. Pulsation spectra of the 36 ZZ Ceti stars in the BG04 ZZ Ceti sample

Object	Class	T _{eff} (K)	log g	Linearly independent modes: Period (s) and Amplitude (mma)										Reference	
BPM30551	cDAV	11260	8.23	920.5 18.5	741.4 21.7	655.4 17.4	442.8 6.5								Hesser et al. 1976
BPM30551	cDAV	11260	8.23	993.0 6.5	936.2 13.0	885.6 15.2	819.2 19.5	738.0 6.5	609.6 6.5						Hesser et al. 1976
BPM30551	cDAV	11260	8.23	963.8 13.0	844.5 19.5	799.2 10.9	682.7 13.0	606.8 13.0							Hesser et al. 1976
BPM30551	cDAV	11260	8.23	920.4 8.7	751.6 13.0	682.7 10.9	606.8 15.2	546.1 5.4	496.5 4.3						Hesser et al. 1976
BPM30551	cDAV	11260	8.23	910.2 8.7	862.3 6.5	731.4 6.5	682.7 13.0	607.9 17.4							Hesser et al. 1976
BPM30551	cDAV	11260	8.23	1129.9 10.9	1057.0 8.7	744.7 18.5	606.8 16.3								Hesser et al. 1976
BPM30551	cDAV	11260	8.23	1137.8 8.7	958.1 7.6	862.3 16.3	744.7 7.6	606.8 14.1							Hesser et al. 1976
BPM30551	cDAV	11260	8.23	1092.3 5.4	993.0 8.7	936.2 9.8	744.7 7.6	712.3 6.5	606.8 11.9						Hesser et al. 1976
BPM30551	cDAV	11260	8.23	862.3 6.5	799.2 8.7	744.7 7.6	668.7 7.6	612.5 5.4							Hesser et al. 1976
R548	hDAV	11990	7.97	333.6 0.6	318.0 0.9	274.8 3.8	274.3 4.8	213.1 7.4	212.8 4.7	187.3 0.9					Mukadam et al. 2003
MCT0145-2211	iDAV	11550	8.14	823.2 17	727.9 19	462.2 25									Fontaine et al. 2003
BPM31594	iDAV	11540	8.11	617.9 48.0	401.6 16	416.1 5									O'Donoghue et al. 1992
HLTau76	iDAV	11450	7.89	933 25.2	796 9.7	781 9.9	541 40.5	494 30.2	383 21.8						Dolez 1998
G38-29	cDAV	11180	7.91	1024.0 26.1	938.0 26.5										McGraw & Robinson 1975
G38-29	cDAV	11180	7.91	1019.8 12.2	910.3 28.3										McGraw & Robinson 1975
G191-16	cDAV	11420	8.05	892.9 100											Vauclair et al. 1989
HS0507+0435B	iDAV	11630	8.17	743.0 13.9	557.7 18.7	446.2 11.0	444.8 13.6	355.8 22.7	354.9 6.8	286.1 3.6					Kotak et al. 2002
HS0507+0435B	iDAV	11630	8.17	743.4 8.3	588.7 3.9	583.8 1.6	559.6 2.7	557.6 17.4	557.2 3.1	556.5 7.8	555.3 18.0	446.1 15.1	445.3 3.0	444.6 12.9	Handler et al. 2002
				355.8 26.1	355.4 4.7	354.9 11.1									
GD66	hDAV	11980	8.05	649.4 2.2	441.9 1.6	301.7 6.7	271.7 8.4	196.5 3.6							Fontaine et al. 1985
GD66	hDAV	11980	8.05	788.6 5.5	461.0 3.6	301.7 6.3	271.7 30	197.2 2.2							Fontaine et al. 1985
GD66	hDAV	11980	8.05	304.5 8.8	271.1 14.8	256.5 9	197.8 7	123.1 2.3							Fontaine et al. 2001
HE0532-5605	iDAV	11560	8.49	688.8 8.3	586.4 7.9										Fontaine et al. 2003
KUV08368+4026	iDAV	11490	8.05	618.0 17.4	494.5 6.0										Vauclair et al. 1997
GD99	cDAV	11820	8.08	1151.0 1.9	1088.0 4.3	1058.0 8.3	1007.0 6.5	976.0 2.1	924.7 1.7	853.2 2.4	633.1 2.0	228.9 4.5	223.6 2.9	105.2 2.0	Chynoweth & Thompson 2005; prv. comm.
G117-B15A	hDAV	11630	7.97	304.4 8.2	271.0 7.3	215.2 23.9									Kepler et al. 1982
KUV11370+4222	hDAV	11890	8.06	462.9 3.5	292.2 2.7	257.2 5.8									Vauclair et al. 1997
G255-2	cDAV	11440	8.17	898.5 9.4	855.4 11.2	819.7 11.3	775.2 15.2	681.2 24.9	607.9 13.1	568.5 6.6					Vauclair 2005; prv. comm.
G255-2	cDAV	11440	8.17	985.2 4.8	773.4 12.7	681.2 27.7	568.5 16.5								Vauclair 2005; prv. comm.
BPM37093	iDAV	11730	8.81	636.7 1.7	633.2 1.1	613.5 1.1	600.7 0.9	582.0 1.0	565.5 1.2	562.6 0.9	548.4 1.1				Kanaan et al. 2005
BPM37093	iDAV	11730	8.81	660.8 0.5	637.2 0.7	633.5 1.3	565.9 0.5	549.2 0.8	531.1 1.2	511.7 0.7					Kanaan et al. 2005
HE1258+0123	cDAV	11410	8.04	1092.1 14	744.6 23	528.5 9									Bergeron et al. 2004
GD154	cDAV	11180	8.15	1190.5 6.3	1186.5 16.7	1183.5 4.6	1092.1 3.0	1088.6 5.0	1084.0 5.6						Pfeiffer et al. 1995
LP133-144	hDAV	11800	7.87	327.3 4	306.9 4	304.5 4	209.2 10								Bergeron et al. 2004
G238-53	hDAV	11890	7.91	206.2 8											Fontaine & Wesemael 1984
EC14012-1446	iDAV	11900	8.16	937 11	610 57	724 21	530 15	399 13							Stobie et al. 1995
GD165	hDAV	11980	8.06	249.7 0.7	192.8 0.9	192.7 2.4	192.6 1.9	166.2 0.4	146.4 0.5	120.4 1.8	120.36 4.8	120.3 1.4	114.3 0.6	107.7 0.4	Bergeron et al. 1993
L19-2	hDAV	12100	8.21	350.1 1.1	348.7 0.5	192.6 6.5	193.1 0.9	192.1 0.8	143.4 0.6	143.0 0.3	118.9 0.3	118.7 1.2	118.5 2.0		Odonoghue & Warner 1982
				114.2 0.3	113.8 2.4	113.3 0.6									
PG1541+651	cDAV	11600	8.10	757 14	689 45	564 15	467 3								Vauclair et al. 2000
R808	cDAV	11160	8.04	833 81											McGraw & Robinson 1976
G226-29	hDAV	12270	8.28	109.5 2.8	109.3 1.1	109.1 2.5									Kepler et al. 1995
BPM24754	cDAV	11070	8.03	1176 22.6											Giovannini et al. 1998
BPM24754	cDAV	11070	8.03	1050 9.1											Giovannini et al. 1998
BPM24754	cDAV	11070	8.03	1086 13.2											Giovannini et al. 1998
BPM24754	cDAV	11070	8.03	978 7.7											Giovannini et al. 1998
BPM24754	cDAV	11070	8.03	1098 6.1											Giovannini et al. 1998
BPM24754	cDAV	11070	8.03	1122 6.7											Giovannini et al. 1998
G207-9	iDAV	11950	8.35	557.4 6.3	318.0 6.4	292.0 5.0	259.1 1.7								Robinson & MacGraw 1976
G185-32	hDAV	12130	8.05	651.7 0.7	537.6 0.6	454.6 0.4	370.2 1.6	301.4 1.1	299.8 1.0	264.2 0.5	215.7 1.9	141.9 1.4	72.9 0.4		Castanheira et al. 2004
G185-32	hDAV	12130	8.05	370.2 1.3	301.6 1.5	215.7 1.9	141.9 1.5	72.6 0.7							Thompson et al. 2004

Table 2—Continued

Object	Class	T_{eff} (K)	$\log g$	Linearly independent modes: Period (s) and Amplitude (mma)														Reference
GD385	hDAV	11710	8.04	256.3 10.9	256.1 11.4													Kepler 1984
GD244	hDAV	11680	8.08	307.0 14	294.6 5.5	256.3 5	203.3 10.5											Fontaine et al. 2001
PG2303+243	cDAV	11480	8.09	900.5 16	794.5 56	675.4 8	623.4 15	570.7 8										Vauclair et al. 1987
G29-38	cDAV	11820	8.14	1015.5 14.5	930.9 25.7	824.7 20.2	677.0 17.6	612.9 20.0										McGraw & Robinson 1975
G29-38	cDAV	11820	8.14	934.5 20.5	813.8 23.5	671.5 23.0	623.8 11.8											McGraw & Robinson 1975
G29-38	cDAV	11820	8.14	859.6 24.6	648.7 7.8	614.3 31.3	498.3 5.8	401.3 4.4	400.4 7.0	399.6 8.8	283.9 3.5							Kleinman 1995
G29-38	cDAV	11820	8.14	915.4 5.9	615.1 58.0	500.4 8.0	474.9 4.8	401.3 5.6	400.4 5.8	399.6 10.0	354.9 2.9	333.9 2.7	283.9 3.5	110.1 0.9				Kleinman 1995
G29-38	cDAV	11820	8.14	770.7 1.5	503.5 8.6	495.0 11.8	401.2 9.7	400.5 1.3	399.7 4.9	283.9 6.4	177.1 0.8							Kleinman 1995
G29-38	cDAV	11820	8.14	809.4 30.1	610.3 10.6	401.2 11.2	399.7 4.5	283.9 6.9										Kleinman 1995
G29-38	cDAV	11820	8.14	894.0 14.0	770.8 8.7	678.4 9.7	612.4 31.6	610.7 8.2	608.9 8.5	551.9 4.4	498.3 6.1	401.2 6.0	399.7 5.7	237.0 1.8				Kleinman 1995
				236.4 1.8														
G30-20	cDAV	11070	7.95	1068 13.8														Mukadam et al. 2002
EC23487-2424	cDAV	11520	8.10	993.0 37.7	989.3 11.0	868.2 12.8	804.5 19.3											Stobie et al. 1993

REFERENCES

- Bergeron, P., et al. 1993, AJ, 106, 1987
- Bergeron, P., Wesemael, F., Lamontagne, R., Fontaine, G., Saffer, R. A., & Allard, N. F. 1995, ApJ, 449, 258
- Bergeron, P., & Lamontagne, R. 2003, NATO ASIB Proc. 105: White Dwarfs, 219
- Bergeron, P., Fontaine, G., Billères, M., Boudreault, S., & Green, E. M. 2004, ApJ, 600, 404
- Brassard, P., Fontaine, G., & Wesemael, F. 1995, ApJS, 96, 545
- Brickhill, A. J. 1992, MNRAS, 259, 529
- Castanheira, B. G., et al. 2004, A&A, 413, 623
- Castanheira, B. G., et al. 2005, A&A, submitted
- Clemens, J. C. 1993, Ph.D. Thesis, University of Texas at Austin
- Cox, J. P. 1980, Research supported by the National Science Foundation Princeton, NJ, Princeton University Press, 1980. 393 p.
- Dolez, N. 1998, Baltic Astronomy, 7, 153
- Dziembowski, W. 1977, Acta Astronomica, 27, 203
- Fleming, T. A., Liebert, J., & Green, R. F. 1986, ApJ, 308, 176
- Fontaine, G., Lacombe, P., McGraw, J. T., Dearborn, D. S. P., & Gustafson, J. 1982, ApJ, 258, 651
- Fontaine, G., & Wesemael, F. 1984, AJ, 89, 1728
- Fontaine, G., Wesemael, F., Bergeron, P., Lacombe, P., Lamontagne, R., & Saumon, D. 1985, ApJ, 294, 339
- Fontaine, G., Bergeron, P., Brassard, P., Billères, M., & Charpinet, S. 2001, ApJ, 557, 792
- Fontaine, G., Bergeron, P., Billères, M., & Charpinet, S. 2003, ApJ, 591, 1184
- Gianninas, A., Bergeron, P., & Fontaine, G. 2005, ApJ, 631, 1100
- Giovannini, O., Kepler, S. O., Kanaan, A., Costa, A. F. M., & Koester, D. 1998, A&A, 329, L13

- Handler, G., Romero-Colmenero, E., & Montgomery, M. H. 2002, MNRAS, 335, 399
- Hansen, C. J., Winget, D. E., & Kawaler, S. D. 1985, ApJ, 297, 544
- Hesser, J. E., Lasker, B. M., & Neupert, H. E. 1976, ApJ, 209, 853
- Kanaan, A., Kepler, S. O., & Winget, D. E. 2002, A&A, 389, 896
- Kanaan, A., et al. 2005, A&A, 432, 219
- Kepler, S. O., Nather, R. E., McGraw, J. T., & Robinson, E. L. 1982, ApJ, 254, 676
- Kepler, S. O. 1984, ApJ, 286, 314
- Kepler, S. O., et al. 1995, ApJ, 447, 874
- Kepler, S. O., Castanheira, B. G., Saraiva, M. F. O., Nitta, A., Kleinman, S. J., Mullally, F., Winget, D. E., & Eisenstein, D. J. 2005, A&A, 442, 629
- Kim, A. et al. 2005, astro-ph/0510104
- Kleinman, S. J. 1995, Ph.D. Thesis, University of Texas at Austin
- Kleinman, S. J. et al. 1998, ApJ, 495, 424
- Kleinman, S. J., et al. 2004, ApJ, 607, 426
- Koester, D., & Vauclair, G. 1997, ASSL Vol. 214: White dwarfs, 429
- Koester, D. & Allard, N. F. 2000, Baltic Astronomy, 9, 119
- Koester, D., & Holberg, J. B. 2001, ASP Conf. Ser. 226: 12th European Workshop on White Dwarfs, 226, 299
- Kotak, R., van Kerkwijk, M. H., & Clemens, J. C. 2002, A&A, 388, 219
- McGraw, J. T., & Robinson, E. L. 1975, ApJ, 200, L89
- McGraw, J. T., & Robinson, E. L. 1976, ApJ, 205, L155
- McGraw, J. T. 1979, ApJ, 229, 203
- McGraw, J. T. 1980, NASA. Goddard Space Flight Center Current Probl. in Stellar Pulsation Instabilities p 501-512 (SEE N80-25229 15-90), 501

- McGraw, J. T., Fontaine, G., Lacombe, P., Dearborn, D. S. P., Gustafson, J., & Starrfield, S. G. 1981, *ApJ*, 250, 349
- Montgomery, M. H. 2005, *ApJ*, 633, 1142
- Mukadam, A. S., Kepler, S. O., Winget, D. E., & Bergeron, P. 2002, *ApJ*, 580, 429
- Mukadam, A. S. et al. 2003, *ApJ*, 594, 961
- Mukadam, A. S., et al. 2004a, *ApJ*, 607, 982
- Mukadam, A. S., Winget, D. E., von Hippel, T., Montgomery, M. H., Kepler, S. O., & Costa, A. F. M. 2004b, *ApJ*, 612, 1052
- Mullally, F., Thompson, S. E., Castanheira, B. G., Winget, D. E., Kepler, S. O., Eisenstein, D. J., Kleinman, S. J., & Nitta, A. 2005, *ApJ*, 625, 966
- Nather, R. E. & Mukadam, A. S. 2004, *ApJ*, 605, 846
- O’Donoghue, D. E., & Warner, B. 1982, *MNRAS*, 200, 563
- O’Donoghue, D., Warner, B., & Cropper, M. 1992, *MNRAS*, 258, 415
- Pesnell, W. D. 1985, *ApJ*, 292, 238
- Pfeiffer, B., et al. 1995, *Baltic Astronomy*, 4, 245
- Robinson, E. L., & MacGraw, J. T. 1976, *ApJ*, 207, L37
- Robinson, E. L. 1979, *IAU Colloq. 53: White Dwarfs and Variable Degenerate Stars*, 343
- Robinson, E. L. 1980, *NASA. Goddard Space Flight Center Current Probl. in Stellar Pulsation Instabilities* p 423-451 (SEE N80-25229 15-90), 423
- Robinson, E. L., Kepler, S. O., & Nather, R. E. 1982, *ApJ*, 259, 219
- Robinson, E. L. et al. 1995, *ApJ*, 438, 908
- Silvotti, R., Voss, B., Bruni, I., Koester, D., Reimers, D., Napiwotzki, R., & Homeier, D. 2005, *A&A*, 443, 195
- Silvotti, R. et al. 2005b, *A&A*, submitted
- Stobie, R. S., Chen, A., O’Donoghue, D., & Kilkenney, D. 1993, *MNRAS*, 263, L13

- Stobie, R. S., O'Donoghue, D., Ashley, R., Koen, C., Chen, A., & Kilkenney, D. 1995, MNRAS, 272, L21
- Thompson, S. E., Clemens, J. C., van Kerkwijk, M. H., O'Brien, M. S., & Koester, D. 2004, ApJ, 610, 1001
- Unno, W., Osaki, Y., Ando, H., Saio, H., & Shibahashi, H. 1989, Nonradial oscillations of stars, Tokyo: University of Tokyo Press, 1989, 2nd ed.
- Vauclair, G., Dolez, N., & Chevreton, M. 1987, A&A, 175, L13
- Vauclair, G., Goupil, M. J., Baglin, A., Auvergne, M. ., & Chevreton, M. 1989, A&A, 215, L17
- Vauclair, G., Dolez, N., Fu, J. N., & Chevreton, M. 1997, A&A, 322, 155
- Vauclair, G., Dolez, N., Fu, J.-N., Homeier, D., Roques, S., Chevreton, M., & Koester, D. 2000, A&A, 355, 291
- Weidemann, V. 1990, ARA&A, 28, 103
- Winget, D. E. 1982, Ph.D. Thesis, University of Rochester
- Winget, D. E. & Fontaine, G. 1982, Pulsations in Classical and Cataclysmic Variable Stars, 46
- Wu, Y. 2001, MNRAS, 323, 248